This document is confidential and is proprietary to the American Chemical Society and its authors. Do not copy or disclose without written permission. If you have received this item in error, notify the sender and delete all copies.

Non-equilibrium molecular dynamics simulations of organic friction modifiers adsorbed on iron oxide surfaces

Journal:	*Langmuir*
Manuscript ID	la-2016-005867.R1
Manuscript Type:	Article
Date Submitted by the Author:	05-Apr-2016
Complete List of Authors:	Ewen, James; Imperial College London, Mechanical Engineering Gattinoni, Chiara; Imperial College London, Mechanical Engineering Morgan, Neal; Shell Global Solutions UK Spikes, Hugh ; Imperial College London, Mechanical Engineering Dini, Daniele; Imperial College London, Mechanical Engineering

SCHOLARONE™
Manuscripts

Non-equilibrium molecular dynamics simulations of organic friction modifiers adsorbed on iron oxide surfaces

James P. Ewen[1]*, Chiara Gattinoni[1], Neal Morgan[2], Hugh A. Spikes[1], Daniele Dini[1]

[1]Imperial College London, [2]Shell Global Solutions, *Corresponding Author: j.ewen14@imperial.ac.uk

Abstract

For the successful development and application of lubricants a full understanding of the nanoscale behavior of complex tribological systems is required, but this is difficult to obtain experimentally. In this study we use non-equilibrium molecular dynamics (NEMD) simulations to examine the atomistic structure and friction properties of commercially relevant organic friction modifier (OFM) monolayers adsorbed on iron oxide surfaces and lubricated by a thin, separating layer of hexadecane. Specifically, acid, amide and glyceride OFMs, with saturated and Z-unsaturated hydrocarbon tail groups, are simulated at various surface coverages and sliding velocities. At low and medium coverage, the OFMs form liquid-like and amorphous monolayers respectively which are significantly interdigitated with the hexadecane lubricant, resulting in relatively high friction coefficients. At high coverage, solid-like monolayers are formed for all of the OFMs which, during sliding, result in slip planes between well-defined OFM and hexadecane layers, yielding a marked reduction in friction coefficient. When present at equal surface coverage, OFMs with saturated and Z-unsaturated tail groups are found to yield similar structure and friction behavior. OFMs with glyceride head groups yield significantly lower friction coefficients than amide and particularly carboxylic acid head groups. For all the OFMs and coverages simulated, the friction coefficient is found to increase linearly with the logarithm of sliding velocity; however, the gradient of this increase depends on the coverage. The structure and friction details obtained from these simulations agree well with experimental results and also shed light on relative tribological performance of these OFMs through nanoscale structural variations. This has important implications in terms of the applicability of NEMD to aid the development of new formulations to control friction.

Introduction

The need for greater energy efficiency in tribological systems has led to a shift towards lower viscosity lubricants, which means that an increasing number of engineering components operate in boundary (thin film) lubrication conditions. As a result, lubricant additives that reduce friction and wear in boundary conditions are of increasing importance[1]. Moreover, with growing concern that engine exhaust after-treatment systems may be poisoned by elements found in some types of friction modifier additives[2], there has been a resurgence of interest in organic friction modifier (OFM) additives which are based solely on C, H, O and N atoms.

OFMs are amphiphilic surfactant molecules that contain a non-polar hydrocarbon tail group attached to a polar head group[3]. The generally accepted friction reduction mechanism involves adsorption of the polar head group to metal or ceramic surfaces, with strong, cumulative Van der Waals forces between proximal non-polar tails leading to the formation of incompressible monolayers that prevent contact between solid surfaces to reduce adhesion and friction[4].

Many different amphiphiles have been tested as OFMs and there are three main structural variables; i) the nature of the head group, ii) the length of the hydrocarbon tail, and iii) the structure of the hydrocarbon tail - whether straight or branched and whether saturated or unsaturated[1]. Early OFMs contained carboxylic acid head groups; however, these were soon found to cause high levels of corrosion for some bearing metals and they were gradually replaced in most applications by less corrosive amphiphiles such as amines, amides, esters or chelating combinations of such groups[1]. Nonetheless, most experimental[3, 4, 5, 6, 7, 8, 9, 10, 11, 12, 13] and simulation[14, 15, 16, 17, 18, 19] tribology studies have utilised OFMs with carboxylic acid head groups. There have been far fewer studies of the more commercially relevant amine[20, 21, 22], amide[9, 23] or glyceride[2, 10] OFMs. Boundary friction experiments have shown that glyceride[10] and amide[9] OFMs can yield lower friction coefficients than their acid counterparts, though the reasons for this were yet to be established prior to this current study. With respect to tail group selection, commercial OFMs generally utilise unbranched aliphatic tail groups

containing 12-20 carbon atoms, due to their effective friction reduction[6], high base oil solubility and availability from natural fats and oils[1]. These natural fats and oils contain mixtures of molecules with saturated as well as mono and polyunsaturated tail groups which are generally used collectively rather than being separated into individual tail group types[1]. The most widely studied components in the literature are saturated C_{18} chains (stearyl) and monounsaturated C_{18} chains with an unsaturated Z-alkene at the C_9 position (oleyl)[1]. Boundary friction experiments at equal concentration showed that OFMs with saturated tails, such as stearic acid and glycerol mono-stearate, gave low friction coefficients which increased linearly with the logarithm of sliding velocity[10]. Conversely, OFMs with Z-unsaturated tails, such as oleic acid and glycerol mono-oleate, yielded significantly higher friction coefficients that remained relatively constant with sliding velocity[10]. One aspect of this current study is to establish whether these observations are due to differences in the nanoscale structure of the film or simply arise from a lower surface coverage at a given concentration due to the 'kinks' from the Z-alkene in the middle of the tail group.

In order to understand how the head and tail group influence the performance of OFMs, it is necessary to obtain a clear picture of: i) the structure of the OFM film and its modification of the interface between the polar metal-oxide surface and the hydrocarbon lubricant, and ii) the effect that this has on the friction coefficient. Detailed structural information of OFM films at the surface–lubricant interface can be obtained from experimental techniques such as sum frequency spectroscopy (SFS)[23], polarized neutron reflectometry (PNR)[11, 20], surface force apparatus (SFA)[8] and in-situ atomic force microscopy (AFM)[13, 22]. These methods can be used to monitor monolayer formation and gather information such as the OFM film thickness and tilt angle. The friction behaviour of OFM films can also be investigated using AFM[13, 22] and SFA[8], as well as dedicated boundary friction experiments[9, 10]. The experimental boundary friction results discussed in this study come mainly from sliding tests using a steel-steel, ball-on-disk contact and a hexadecane solvent[10]. These tests employ low sliding velocities (mm s^{-1}) and high pressures (GPa) in order to minimise lubricant entrainment and thus maintain boundary lubrication conditions.

Classical molecular dynamics simulations can be used to simultaneously probe the nanoscale structure and friction of OFM films[16, 21], making it a valuable complement to experiments. The use of well-tested all-atom force fields yields an accurate representation of the structure of large systems (tens of thousands of atoms), where the collective behavior of many OFM molecules can be reliably analysed over time. Moreover, non-equilibrium molecular dynamics (NEMD) simulations can provide important information on the frictional behavior of the system under a range of conditions. Indeed, NEMD simulations have provided unique insights into the friction behavior of a multitude of systems; from alkylsilane monolayers on silica surfaces[24], to diamond-like carbon (DLC) coatings[25] and platinum AFM tips on gold surfaces[26]. Previous NEMD simulations of OFM monolayers have analysed the film structure and friction of acid[16] and amine[21] OFMs using reasonably thick lubricant films, low pressures (P_z = 0.1 GPa) and relatively low coverages. NEMD simulations have also been used to quantify the Derjaguin offset in high coverage carboxylic acid films both in intimate contact, and separated by a thin layer of lubricant[15]. It has been suggested from these simulations that OFM monolayers with that are less interdigitated[16] and smoother[15] yield lower friction coefficients. However, the specifics of how OFM film structure and friction change with molecular structure, coverage and sliding velocity are yet to be fully explored in systems with thin lubricant films under high pressure (P_z = 0.5 GPa) as used in boundary friction experiments[10].

Thus the aim of the current study is to use NEMD simulations to shed light on the nanoscale structure of OFM films adsorbed on iron oxide surfaces and separated by a thin layer of hexadecane, to calculate the friction coefficient as a function of coverage and sliding velocity, and to fully explore links between the structure and friction. A wide range of OFMs are explored in order to better understand the influence of head group type and tail group Z-unsaturation on structure and friction (Figure 1-b). In addition, the use of OFM films with a wide range of coverages, including close to the theoretical limit, should indicate the significance of the formation of close-packed monolayer films in the reduction of boundary friction. The velocity-dependence of the friction coefficient for different OFMs and coverages will also be analysed and compared to boundary friction experiments. The

structure of the remainder of this publication will now be outlined. First, the general system set up for all of the simulations is introduced, followed by the specific methodology for the preliminary squeeze-out and compression and sliding simulations. This is followed by the results of the preliminary squeeze out simulations and finally the structure and friction results from the compression and sliding simulations are discussed in detail.

Methodology

System Setup

A representative example of the systems simulated in this study is shown in Figure 1-a. It consists of a thin layer of hexadecane lubricant confined between two OFM monolayers adsorbed on iron oxide slabs. All structures were constructed using the Materials and Processes Simulations Platform (MAPS) from Scienomics SARL. Three different OFM head groups (carboxylic acid, amide, glyceride) and two different tail groups (stearyl, oleyl) are considered in these simulations. Acid OFMs were selected to allow comparison to previous experiments and simulations, while amide and glyceride OFMs are more commercially relevant[1]. Specifically, NEMD simulations were used to compare the structure and friction of stearic acid (SA), oleic acid (OA), stearic amide (SAm), oleamide (OAm), glycerol mono-stearate (GMS) and glycerol mono-oleate (GMO) films at a range of surface coverages and sliding velocities (Figure 1-b). Hexadecane was chosen as a model base oil because its properties are well defined, and it is commonly employed in both experimental[10, 13, 22] and modelling[15, 16, 21] tribology studies. Given that charge separation is unfavourable in the low-polarity hexadecane solvent, all OFM molecules were assumed to be in their electronically neutral form.

Classical MD simulations were performed using LAMMPS[27]. In all of the MD simulations, (100) slabs of α-iron(III)-oxide[28] (hematite) with dimensions (*xyz*) of approximately 55 Å × 55 Å x 12 Å were used as the substrates, representing a single asperity contact. Periodic boundary conditions were applied in the *x* and *y* directions. Care was taken to cleave the surface in a manner such that the Fe:O ratio remained at 2:3, in order to ensure that surfaces with no overall charge were produced. OFM molecules were oriented perpendicular to, and initially 3 Å from, the interior surfaces of two such

slabs (Figure 1-a). This produced OFM films similar to those formed by the Langmuir-Blodgett experimental procedure, see *e.g.* Ref. [5]. Hexadecane molecules were then randomly distributed between the OFM films.

If one assumes a mono-dentate binding mode for the glycerides, the limiting head group area for all of the OFMs is around 22 Å^2 [2, 29]. The surface coverage or packing density can be quantified as the number of head groups per area of surface, Γ. A high surface coverage (Γ = 4.32 nm^{-2}), close to the maximum theoretical value[29], is simulated by adsorbing 132 OFM molecules on each 3000 Å^2 slab to form a close-packed monolayer. Two other surface coverages are considered: a medium coverage (Γ = 2.88nm^{-2}), approximately 2/3 of the maximum coverage; and a low coverage (Γ = 1.44 nm^{-2}), around 1/3 of the maximum coverage. The high coverage simulated has been achieved experimentally on steel surfaces for acids and amides[29], but not reported for glycerides. However, previous MD simulations[2] as well as experimental results at the air-water interface[30] suggest that the high coverage employed should also be possible for glycerides. In tribology experiments, OFM concentration in the lubricant is generally used rather than surface coverage since it is far easier to measure and control. PNR experiments of palmitic acid[11] suggest that at intermediate concentrations (150-1000 ppm), surface coverage increases linearly with OFM concentration in the lubricant. However, in order to directly compare OFM concentration and coverage, more research is required to understand how the coverage asymptotes at lower and higher concentrations for the specific molecules studied here.

A combination of several updated versions of the OPLS all-atom force-field[31] were used to represent both hexadecane and the OFM molecules; full details and original references can be found in the supporting information. The OPLS family of force-fields was chosen for three main reasons; i) the inclusion of specific parameters for all of the functional groups required[31, 32], ii) all-atom representation expected to be critical in accurately modelling friction in this system (quantitative comparisons to be published separately), iii) recent parameterizations available which allow far

more accurate representations of long-chain hydrocarbon than previously possible[33]. The final point is critical since the original OPLS parameterization has been shown to misrepresent the liquid-solid phase behavior of long-chain alkanes[33, 34]; an issue which would certainly impact the behavior observed in these simulations. Lennard-Jones interactions were cut-off at 10 Å[34] and 'unlike' interactions were evaluated using the geometric mean mixing rules, as prescribed in the OPLS force-field[31]. Electrostatic interactions were not cut-off, but rather evaluated using a slab implementation of the PPPM algorithm[35].

Surface-lubricant and surface-OFM interactions are represented by the Lennard-Jones and Coulomb potentials; the hematite surface parameters selected are those developed by Berro *et al.*[36], which are outlined in the supporting information. DFT calculations are also being conducted to better understand the nature and strength of the surface-OFM interactions. The hematite surface atoms were restrained in the corundum crystal structure by harmonic bonds between surface atoms within 3 Å. The force constant of these bonds was chosen to be 130 kcal mol^{-1} $Å^{-2}$, which has been shown previously to keep the surface structure suitably rigid, but not to adversely affect the thermostatting[36]. It is worth noting that in previous MD simulations of the adsorption of similar molecules onto hematite surfaces the adsorption energy was dominated by the long-range electrostatic contribution between the head group and the polar surface[14].

The MD equations of motion were integrated using the velocity-Verlet algorithm with an integration time-step of 1.0 fs. Fast-moving bonds involving hydrogen atoms were constrained with the SHAKE algorithm[37]. The Langevin thermostat[38], with a time relaxation constant of 0.1 ps was used in all of the simulations in order to maintain a temperature, T = 300 K. The pressure (P_z = 0.5 GPa) was controlled by applying a constant normal force to the outermost layer of atoms in the upper slab, keeping the *z*-coordinates of the outermost layer of atoms in the lower slab fixed, as previously proposed[16, 39] (Figure 1-a).

Preliminary Squeeze-Out Simulations

In order to estimate the thickness of the central hexadecane film under the applied pressure, preliminary squeeze-out simulations were performed prior to the compression and sliding simulations. Previous simulations[40, 41] and AFM experiments[42] of hydrocarbon squeeze-out between solid surfaces showed that there was an energy barrier to overcome when removing sufficient fluid to result in one fewer molecular layer. The size of this barrier increased both when longer chains with a higher viscosity were used and also increased progressively when fewer molecular layers remained in the contact[40, 41, 42]. Hence, a relatively large pressure was required to squeeze out the last few molecular layers of fluid. From these previous results, it was expected that an equilibrium thickness of between 1 and 3 molecular layers of hexadecane would remain in the contact under the simulation conditions (P_z = 0.5 GPa, T = 300 K).

Starting from the system described above, 50 Å of vacuum was added in the *x* and *y* directions to allow hexadecane molecules to be squeezed out of the contact, while the strongly adsorbed OFM molecules remained on the surface. Periodic boundary conditions were maintained outside of this extended system. At this stage the thermostat was applied to the entire system. Two-hundred hexadecane molecules were randomly distributed between the OFM-covered slabs, corresponding to roughly five molecular layers for this contact area (≈3000 $Å^2$). The slabs were moved closer together by applying a velocity (10 m s^{-1}) to the top slab until the density of the OFM and hexadecane region was similar to that of liquid hexadecane (0.75 g cm^{-3}) and the system was then energy minimised. Pressure (P_z = 0.5 GPa) was then applied until the average slab separation reached equilibrium, after approximately 250 ps (Figure 2-a). The number of hexadecane molecules remaining in the contact was estimated by dividing the number of hexadecane carbon atoms between the slabs by sixteen. This residual number of hexadecane molecules was used for the following compression and sliding simulations.

The addition of the vacuum to the edge of the system may mean that so-called finite-size effects[43] influence the residual number of hexadecane molecules. Therefore, squeeze-out simulations were

also conducted with system sizes two and four times as large as those used in the compression and sliding simulations to ensure consistency. Indeed, the squeeze-out data presented in the results and discussion section scaled well with system size, with the same number of hexadecane layers remaining inside the contact in the larger systems (supporting information).

Compression and Sliding Simulations

The compression and sliding simulations used systems containing the residual number of hexadecane molecules from the squeeze-out simulations, with the same three coverages of OFM molecules as outlined previously, but with the vacuum in the *x* and *y* directions removed. A density similar to that of liquid hexadecane (0.75 g cm^{-3}) was reached by moving the top slab down at 10 m s^{-1} prior to energy minimisation. The system was then pressurised (P_z = 0.5 GPa), thermostatted in the directions perpendicular to the compression (*x* and *y*), and allowed to equilibrate at 300 K. Initially, the slab separation varied in a damped harmonic manner, so sliding was not applied until a constant average slab separation was obtained and the hydrostatic pressure within the hexadecane film was close to its target value[36]. These compression simulations were generally around 200 ps in duration. During the compression stage, there was a collective tilting of the OFM molecules towards the surface in a random direction. The sliding direction (*x*) was chosen to be perpendicular to the orientation of this initial tilt (*y*). Previous NEMD simulations of monolayers in intimate contact, with the tilt orientated parallel to the sliding direction (*x*) have shown high friction and stick-slip behaviour due to the high commensurability of the interface[15, 44]. However, the presence of a thin, separating layer of hexadecane in previous NEMD simulations has been shown to maintain low friction[15]. Hence the consistently low friction observed in boundary friction experiments[10] is expected to be reproduced in these simulations due to the presence of the hexadecane layer between the OFM films. Additional simulations with the sliding direction completely aligned with the initial tilt were also conducted to confirm that the initial orientation of the tilt did not influence the friction results obtained.

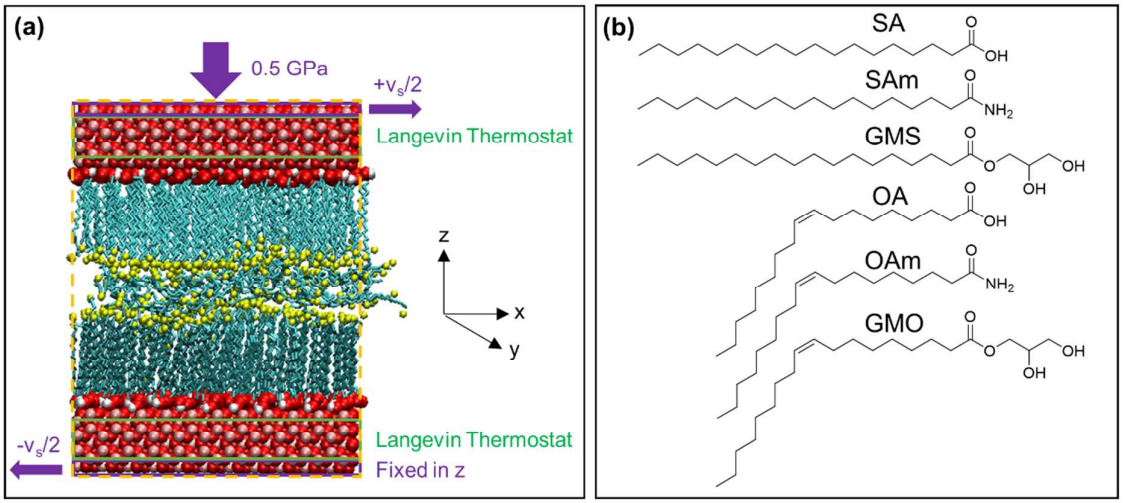


Figure 1. Simulation details: setup for compression and sliding simulations (a). Example shown for SA at high coverage after compression, before sliding. Head groups are shown with O in red and H in white, terminal C in yellow and the other tail group C in cyan. Hydrogen atoms in the tail groups are omitted for clarity. In the slab, Fe atoms are shown in pink. Periodic boundary conditions (yellow dotted line) applied in *x* and *y*. Rendered using VMD[45]. Chemical structures of OFMs simulated in this study (b); stearic acid (SA), stearic amide (SAm), glycerol mono-stearate (GMS), oleic acid (OA), oleamide (OAm) and glycerol mono-oleate (GMO).

After compressive oscillation became negligible, a velocity of $v_x = \pm v_s/2$ was added in the *x* direction to the outermost layer of atoms in each slab (Figure 1-a) and sliding simulations were conducted for 0.5-10 ns, depending on the sliding velocity. The values of v_s applied were 1, 2, 5, 10 and 20 m s^{-1} and all simulations were run for long enough to yield a sufficient sliding distance (10 nm) to obtain representative values for the friction coefficients (uncertainty <10%). While lower sliding velocities are desirable to match those used in boundary friction experiments (typically mm s^{-1}), they are not yet accessible using all-atom NEMD simulations of this scale[16]. During the sliding simulations, any heat generated was dissipated using a thermostat acting only on the middle 10 Å of both iron oxide slabs (Figure 1-a), applied in the direction perpendicular to the both the sliding and compression (*y*)[46]. This is known to be advantageous over direct thermostatting of the fluid which has been shown

to significantly affect the behaviour of confined fluids under sliding conditions[47]. The boundary thermostatting method applied here has been shown previously to be effective in controlling the temperature of similar systems and sliding velocities[48]. At the onset of sliding, an expansion due to the increase of temperature by shear heating was expected so it was ensured that steady state sliding had been attained before sampling began for the friction coeffiecient[36]. The time taken to achieve steady state sliding decreased with increasing sliding velocity but always equated to approximately 2 nm of sliding distance.

The kinetic friction coefficient, μ, was obtained using the extended Amontons−Coulomb law under the high load approximation[16]: $F_L/F_N = F_0/F_N + \mu \simeq \mu$. F_L and F_N are respectively the average total lateral and normal forces acting on each slab, and F_0 is the load-independent Derjaguin offset, representing adhesive surface forces. The validity of this approximation was confirmed for two test cases (SA, GMO) by ensuring that a linear fit of F_L as a function of F_N gave an insignificant value of F_0, and the same result for μ within the statistical uncertainties. An insignificant value of F_0 was expected from previous simulations which included a thin layer of lubricant confined between the monolayers[15]. In general, the assumption $\mu \simeq F_L/F_N$ is appropriate for systems with low adhesion (small F_0) or under high applied loads (large F_N)[49]; both of these are applicable to these simulations.

Results and Discussion

The results are presented as follows. Results of the preliminary squeeze-out simulations are outlined first. This is followed by a detailed analysis of the structure of the film at different coverages under sliding conditions. The friction results at different coverages and sliding velocities are then described and linked to the structural variations in the films. In what follows, some properties are expressed as functions of the distance from the surface, denoted by *z*; this is taken as the distance from the innermost layer of atoms on the bottom slab.

Preliminary Squeeze-Out Simulations

Simulations to establish the appropriate thickness of a boundary film of hexadecane under high pressure (P_z = 0.5 GPa) were performed first. The variation of the overall slab separation and of the number of confined hexadecane molecules from the beginning of the simulation is shown for a representative OFM (SA) in Figure 2. As expected, the slab separation distance (Figure 2-a) decreases asymptotically to reach an equilibrium value[41]. Changes in gradient due to layer-layer transitions[41] are most easily observed at low coverage, where the deformation of the OFM has a less significant effect on the change in slab separation than at medium and high coverage. The equilibrium slab separation decreases from 30 Å at high coverage, to 20 Å at low coverage. All of the OFM films deform considerably, leading to significantly thinner equilibrium slab separations than those found in subsequent compression and sliding simulations, where no vacuum is present in the *x* or *y* directions.

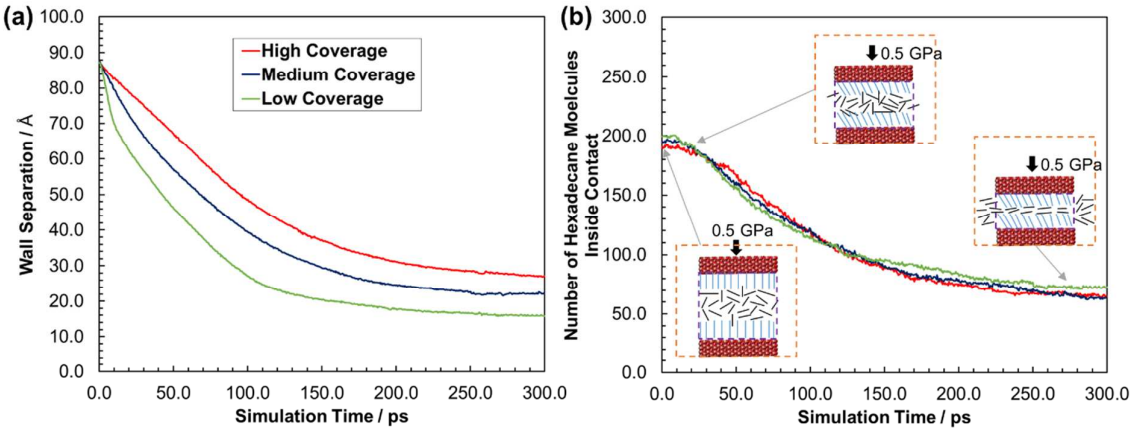


Figure 2. Results of squeeze-out simulations for representative OFM (SA) at different coverages: variation in the slab separation (a) and the number of hexadecane molecules within contact volume (b), over 300 ps, P_z = 0.5 GPa. Inset schematics in (b) show the sturcture of the initial system, followed by compression of OFM film and squeeze-out of hexadecane. Blue lines represent OFM molecules, black lines represent hexadecane. Orange dotted line shows periodic boundaries, purple dotted line shows contact volume.

Figure 2-b shows how the number of hexadecane molecules inside the contact volume decreases with time. Before 25 ps there is little change in this value as the OFM film is compressed, after this point the number of molecules decreases asymptotically as expected[41]. The number of hexadecane molecules stabilises at around 70 at all coverages, which corresponds to approximately two horizontally-oriented molecular layers. Thus these simulations suggest that the equilibrium number of hexadecane molecules remaining inside the contact volume is essentially independent of OFM coverage. This two-layer limit agrees well with extrapolations from previous squeeze-out simulations for C_3-C_{14} hydrocarbons between gold surfaces[40] as well as experimental AFM data for hexadecane between graphite surfaces which suggest that the 2→1 layer transition only occurs above 0.6 GPa[42]. These results did not vary significantly between the different types of OFM, so the subsequent compression and sliding simulations were based on systems containing 70 hexadecane lubricant molecules (two molecular layers) for all types and coverages of OFM.

Structure during Sliding

Classical MD simulations of the OFM-hexadecane system under sliding conditions can yield important information regarding both the atomistic structure of the confined films and their friction behavior. Figure 3 shows simulation snapshots for a representative OFM (SA) at low, medium and high surface coverages after 500 ps of sliding at 10 m s^{-1}.

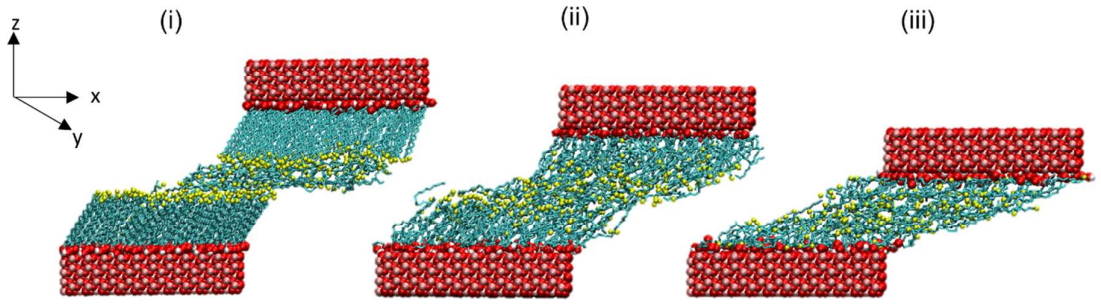


Figure 3. Simulation snapshots of representative OFM (SA) after 500 ps of sliding at: high coverage (i), medium coverage (ii), and low coverage (iii), P_z = 0.5 GPa, v_s = 10 m s^{-1}. Oxygen atoms are shown in red, head group hydrogen atoms in white, terminal carbon atoms in yellow, the other tail group carbon atoms in cyan and iron atoms in pink. Hydrogen atoms in the tail groups are omitted for clarity. Periodic images and boundaries are not shown. Rendered using VMD[45].

The structure of the confined films has been studied under sliding conditions (v_s = 10 m s^{-1}) by analysing their atomic mass density profile (Figure 4), atomic position probability profile (Figure 5), radial distribution function (Figure 6), hydrogen-bonding network (Figure 7), velocity profile (Figure 8) and centre of mass and tilt angle (Figure 9). In general, the structure of the films remains very similar after the compression phase and during the sliding phase (supporting information), which is consistent with previous NEMD simulations[16, 21, 50]. However, the film structure changes significantly with OFM coverage and to a much lesser extent between different head groups and tail groups.

The overall thickness and layering of the system in the z direction, as well as the interdigitation of the OFM and hexadecane layers, can be observed through mass density profiles, ρ(*z*) (Figure 4) and atom position probability profiles, p(*z*) (Figure 5). Data are shown for the saturated and unsaturated acids (SA, OA) and glycerides (GMS, GMO); amides (SAm, OAm) are an intermediate case between the two other head groups, so data for them are shown in the supporting information.

Sharp, intense peaks at the far left and right-hand side of Figure 4 indicate adsorption of OFM head groups on the surface, whilst the less intense peaks which extend further from the surface are due to the tail groups. The OFMs films become substantially thicker and more structured with increasing

coverage. At high coverage (Γ = 4.32 nm^{-2}), the slabs are separated by approximately 50-55 Å, with up to ten small peaks which indicate layering of the tail group carbon atoms. Comparing profiles from OFMs with stearyl (solid) and oleyl (dotted) tail groups, it is clear that the presence of Z-unsaturation does not significantly alter the peak positions or slab separations. The high coverage slab separations agree well with SFA experimental observations, which found that SA films on opposing mica surfaces in hexadecane (46-54 Å) were of similar thickness to those formed by OA (50-55 Å) when an elevated concentration of OA was used[8]. At medium coverage (Γ = 2.88 nm^{-2}), the slabs are separated by approximately 40 Å and the OFM tail groups show much less layering. At low coverage (Γ = 1.44 nm^{-2}), the slabs are separated by just 25 Å and the OFM displays only two clear peaks; a large peak at the surface incorporating both the head group and tail group atoms close to the surface, and a smaller peak which extends to approximately 5 Å from the surface. The slab separation is greater for glycerides (Figure 4-a) than acids (Figure 4-b) and amides as a result of the larger head group size, with the greatest difference being at high coverage (5 Å).

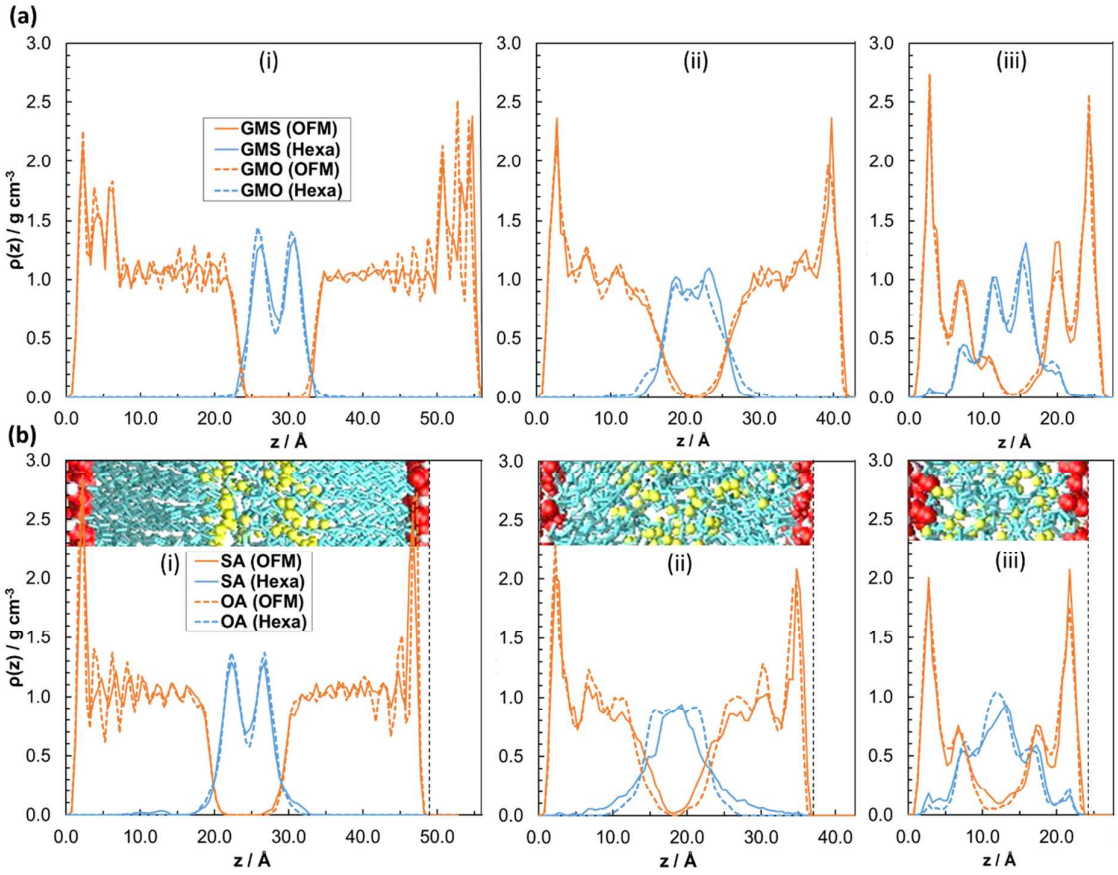


Figure 4. Atomic mass density profiles in *z*, ρ(*z*), of OFM (orange) and hexadecane (blue) for (a) glyceride (GMS, GMO) and (b) carboxylic acid (SA, OA) head groups with stearyl (solid) and oleyl (dotted) tail groups at high (i), medium (ii) and low (iii) coverages. The vertical black dotted line in (b) shows the positon of the top slab. Profiles for amides (SAm, OAm) as well as those under compression conditions are shown in the supporting information. Image overlay shows section of SA OFM film at corresponding coverages to help to illustrate the interdigitation.

The height of the individual OFM films can be estimated by measuring the distance of the terminal carbon in the OFM tail, CTT, from the surface, as shown in Figure 5. At high surface coverage, glyceride film heights are approximately 21 Å (Figure 5-a-i), while for acids (Figure 5-b-i) and amides they are closer to 19 Å, which agrees well with experimentally measured film thicknesses from in-situ AFM experiments[13]. At medium coverage, the average position of the OFM CTT peak is broader

and shifted slightly closer to the surface (approximately 12 Å). At low surface coverage, there are two sharper OFM CTT peaks at just 2 and 7 Å from the surface.

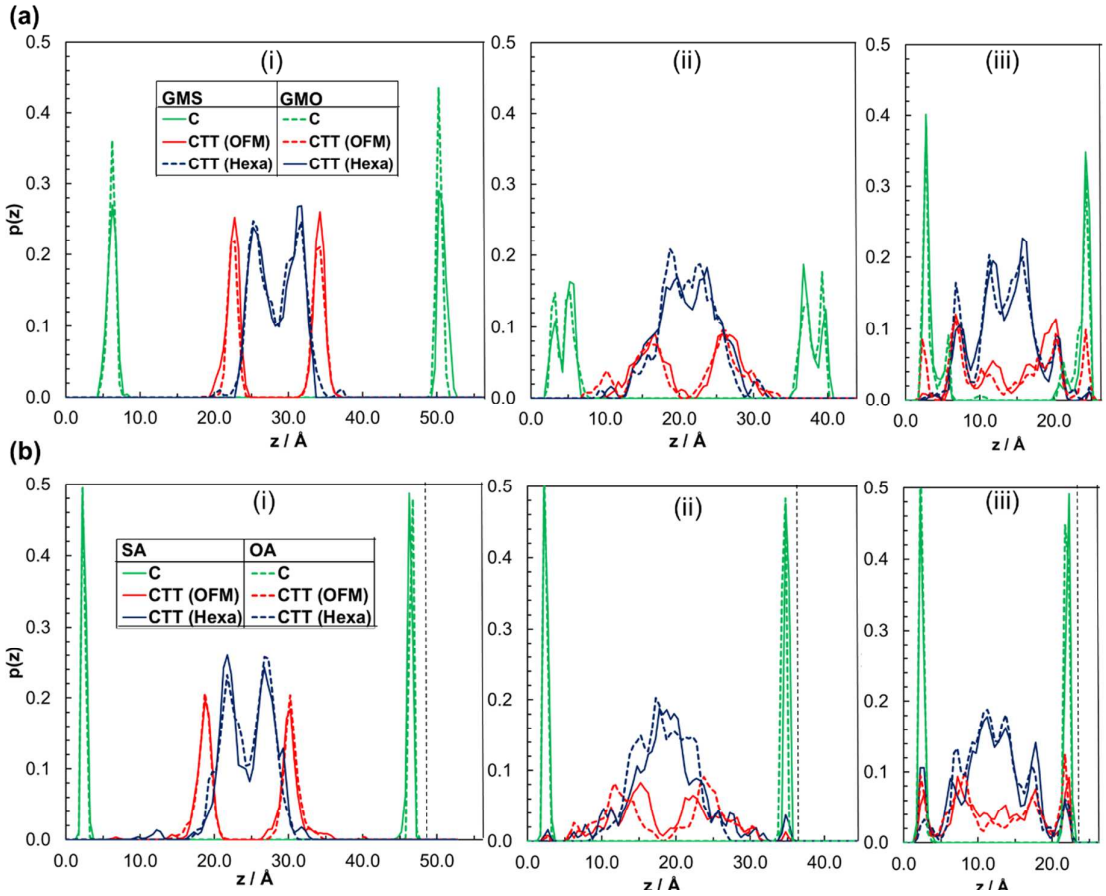


Figure 5. Atomic position probability profiles in *z*, p(*z*), for carbonyl C (green), hexadecane terminal CTT (blue) and OFM terminal CTT (red) atoms in GMS and GMO (a) SA and OA (b), at high (i), medium (ii) and low (iii) coverage. Profiles for other OFMs are shown in the supporting information. The vertical black dotted line in (b) shows the positon of the top slab.

The intense carbonyl, C, peaks close to the surface in Figure 5 indicate that the head group positions are also localised in *z*. At low coverage, the C peaks are only 2 Å from the surface for all of the OFMs. For glyceride OFMs (Figure 5-a), this suggests that most head groups are bound in a bidentate mode, with both alcohol groups bound to the surface. At medium coverage, the glyceride C profiles are significantly different to those for acids and amides, with a second peak of equal intensity appearing

at 5 Å from the surface. This suggests that, at medium coverage, around half of the molecules are bound in a bidentate mode with the C atoms close to the surface, and half are bound in a monodentate mode with C atoms further from the surface. For high coverage glyceride films there is only a peak at 5 Å, suggesting that all molecules are now bound in a monodentate mode. The C peaks for acids (Figure 5-b) and amides are generally far sharper than for glycerides (Figure 5-a) due to the closer proximity of the C atoms to the surface.

Figure 4 and 5 also reveal important information regarding the level of interdigitation of the OFM films and the hexadecane lubricant, which is indicated by the penetration of the hexadecane profile into the OFM profile. The amount of penetration is influenced significantly by both the coverage and the head group type. For all of the OFMs tested, at high coverage two distinct hexadecane peaks form which correspond to well-separated layers. In Figures 4 and 5, the outer limits of the hexadecane peaks only extend to around 1 Å into the OFM peaks for glycerides (a-i), which increases to 3 Å for acids (b-i) indicating more interdigitation for the latter. At medium coverage, there is less layering of the lubricant, with only one broad hexadecane peak, the outer limits of which extend much further into the OFM film; 5 Å for glycerides (a-ii), 10 Å for acids (b-ii). At low coverage, there is even more penetration of the hexadecane and OFM profiles, with a non-zero value for the OFMs in the centre of the film, indicating that films on opposing slabs are directly interdigitated. In fact, at low coverage the hexadecane and OFM peaks directly overlap, suggesting that they form mixed layers; which are likely to behave similarly to thin films of pure hexadecane[51]. The glyceride profiles at low coverage (a-iii) contain a higher number of better defined peaks than those for acids (b-iii) and amides (6 vs. 5), suggesting more numerous, well-separated layers.

The ordering within the OFM films was examined further by calculating separate radial distribution functions (RDFs), g(r), for the head group carbon (C), and the terminal carbon (CTT). In Figure 6, the C RDFs are shifted upwards by 10 units for clarity.

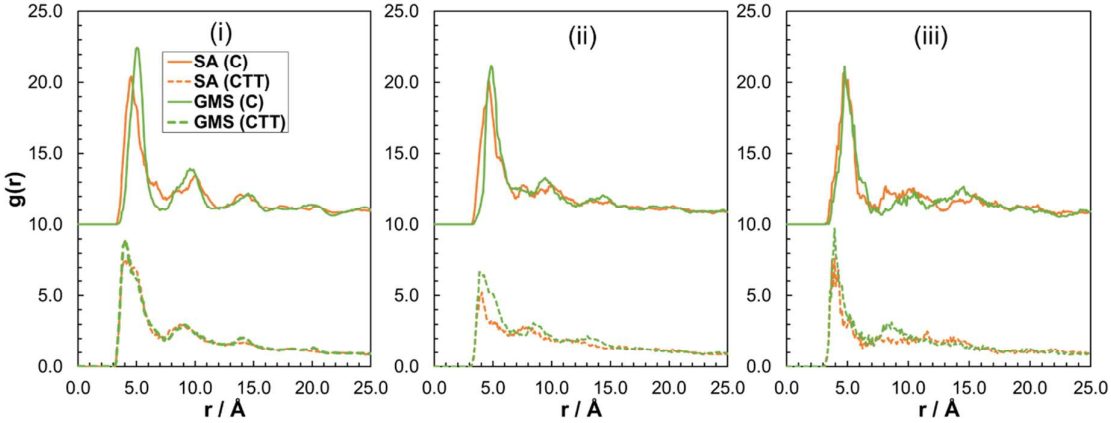


Figure 6. Radial Distribution Function (RDF) describes the ordering of the terminal CTT (dotted) and carbonyl C (solid) atoms for SA (orange) and GMS (green) at high (i), medium (ii), and low (iii) coverage. The C RDFs are shifted upwards by 10 units for clarity.

In Figure 6, the carbonyl carbon, C, shows long-range order for all OFMs and coverages, with the major peaks occurring at multiples of r = 5 Å. This corresponds to the unit-cell dimension of the hematite surface[28], confirming that the surface dictates the head group packing in the OFM films[16]. Whilst the C peak at 5 Å is of similar intensity at all coverages, at high coverage, there are sharper peaks at 10, 15 and 20 Å, indicating increased long-range ordering and more solid-like films. At all coverages, the terminal CTT peaks are at least 25% less intense than the carbonyl C peaks, suggesting that the tail group positions are less ordered. However, at high coverage, there are still identifiable CTT peaks at 10, 15 and 20 Å, suggesting that the films remain solid-like at the interface between the OFM film and the hexadecane lubricant. At medium coverage, all of the CTT peaks are less sharp and intense than at high coverage, suggesting that the film is more amorphous with less correlation between the carbonyl and terminal carbon positions. At low coverage, the CTT peak at 5 Å is more intense than at medium coverage because the terminal carbon atoms are close enough to the surface such that it influences their packing. Overall there appears to be a correlation between the intensity and long-range order of C and CTT peaks, suggesting that more ordered head group atoms can lead to more ordered tail group atoms. The peaks for GMS (Figure 6-a) are generally sharper and more intense than those for SA (Figure 6-b) at all coverages, suggesting that the former

yields more ordered, solid-like films. OFMs with amide head groups represent an intermediate case between acid and glyceride head groups.

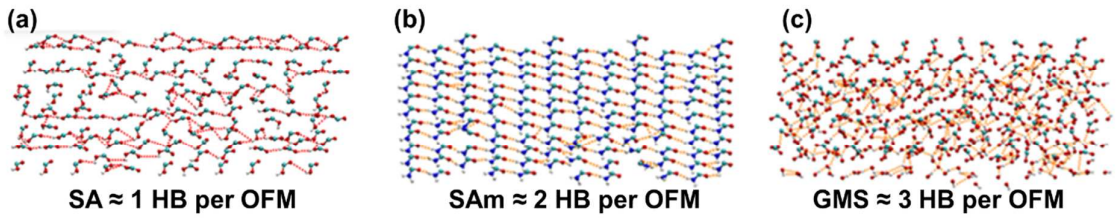


Figure 7. Snapshots of hydrogen-bonding between OFM head groups at high coverage 500 ps into sliding simulation: SA (a), SAm (b) and GMS (c). Head groups: oxygen shown in red, hydrogen in white, nitrogen in blue and carbon in cyan, tail groups omitted for clarity, hydrogen-bonds[52] shown in orange.

The differences in the phase of and levels of interdigitation between films formed from different OFM head groups is postulated to be due to variations in the hydrogen-bonded networks, which are shown for the high coverage case in Figure 7. These networks were analysed in VMD[45] using standard criteria for hydrogen-bonding[52], *i.e.* a bond length cut-off of 3.9 Å, and an angle cut-off of 90°. Intermolecular hydrogen-bonding between the head groups appears to have an effect on the structure of the OFM-lubricant interface, through inducing a more solid-like film in glycerides than in acids. Amide OFMs are an intermediate case between acid and glyceride OFMs. Indeed, excluding those formed between the OFM and the surface, high coverage GMS films contain approximately three intramolecular hydrogen-bonds per molecule; SAm two such bonds per molecule; and SA one per molecule. The presence of unsaturation in the tail group has no effect for acid or amide OFMs; however, GMO only forms approximately two hydrogen-bonds per molecule, perhaps explaining the greater levels of interdigitation in its films compared to GMS.

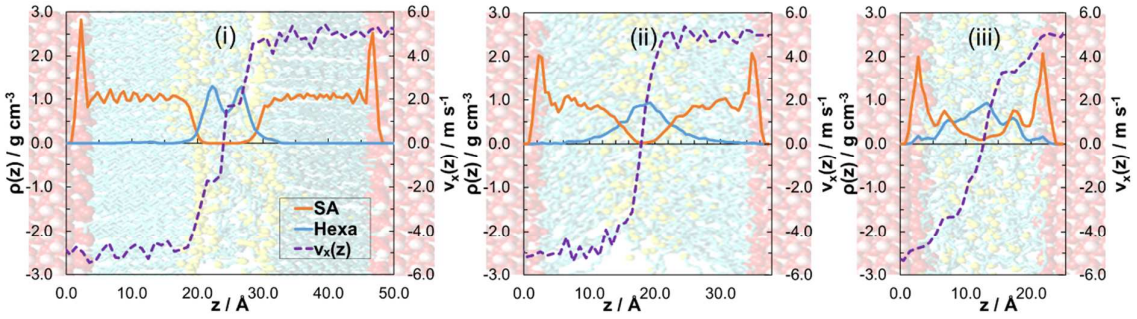


Figure 8. Profile of atom *x* velocities from 0.5 Å spatial bins in *z*, $v_x(z)$, overlaid on to mass density profile, ρ(z), and a snapshot of representative OFM system (SA) at high (i), medium (ii) and low (iii) coverage. P_z = 0.5 GPa, v_s = 10 m s^{-1}.

In order to understand flow within the confined films during sliding, velocity profiles, $v_x(z)$, for a representative OFM (SA) are shown in Figure 8. Velocity profiles are overlaid onto mass density profiles, ρ(z), and a snapshot of the system in order to aid interpretation of the results. Atom velocities are computed for 0.5 Å spatial bins which are averaged over 100 ps time blocks during the sliding phase. The velocity profiles at all coverages show that there is no slip at the surface, as expected for the strongly absorbed OFM head groups. The OFM tail groups move at a similar velocity as the slab to which they are absorbed (±5 m s^{-1}) until the region where they become interdigitated with the hexadecane lubricant. For SA at high coverage (i), these interfaces are at approximately 20 Å and 28 Å, at which points the gradient increases as the interface is sheared. At 22 Å and 26 Å, there is a flattening of the velocity profile, corresponding to the two hexadecane peaks in the mass density profile, with another increase in velocity gradient at 24 Å between the two hexadecane layers. This suggests that these two hexadecane layers move as 'plugs' between the OFM films, with three separate slip planes, *i.e.* at the OFM-hexadecane interfaces as well as between the two hexadecane layers. At medium coverage (ii), the slip plane becomes more difficult to define, and there appears to be significant shearing within the portion of the OFM tail group which is interdigitated with hexadecane. The velocity profile passes through zero at the centre of the hexadecane layer, with a shallower gradient than at high coverage. The low coverage velocity profile (iii) is more typical of conventional planar Couette flow, with a near linear velocity profile of the

liquid between the slabs. However, the velocity profile still contains steps which indicate partial plug-flow between combined OFM-hexadecane layers. Such stepped velocity profiles have also been observed in previous NEMD simulations of pure hexadecane films of similar thickness[52].

The extension and orientation of the OFM films during sliding are further analysed by calculating the average centre-of-mass with respect to the *z* coordinate, z_{CoM} (Figure 9-a) and also the tilt angle, θ, defined as the angle between a vector from the carbonyl C atom to the carbon atom halfway up the chain (C_9) and the surface normal (Figure 9-b).

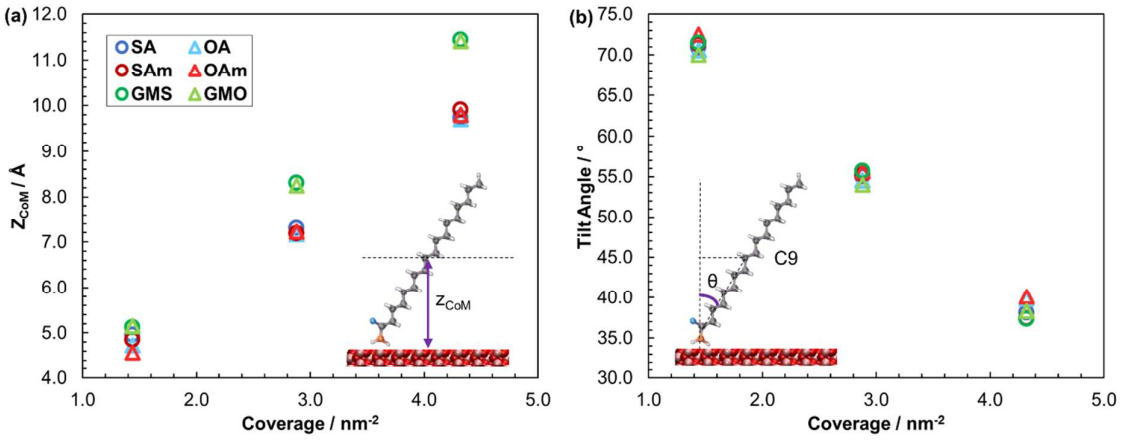


Figure 9. OFM film extension and orientation: average z_{CoM} of OFMs as a function of coverage (a), average $C_{1\text{-}9}$ tilt angle as a function of coverage under sliding conditions (b), P_z = 0.5 GPa, v = 10 m s^{-1}. Error bars not shown as within size of symbol. Circles represent OFMs with saturated tail groups, triangles represent OFMs with tail group Z-unsaturation.

At low coverage z_{CoM} ≈ 5 Å and θ ≈ 70°, indicating that most molecules are lying almost flat to the surface. z_{CoM} increases linearly with coverage, at two different gradients depending on the head group. For acid (SA, OA) and amide (SAm, OAm) head groups, the z_{CoM} reaches a maximum of approximately 10 Å at high coverage, while for glyceride head groups, the maximum is 11.5 Å due to the larger head group size. This means that, for the same tail group, glyceride OFMs yield slightly thicker films than acids or amides. OFMs with saturated and Z-unsaturated tail groups have similar values for the z_{CoM}, though saturated films are very slightly more extended (<0.2 Å). The tilt angle, θ,

decreases linearly with coverage at the same rate for all of the OFMs, to approximately 55° at medium coverage, and 40° at high coverage. The high coverage value agrees reasonably well with tilt angles estimated from in-situ AFM experiments, around 50° for SA[13] and stearyl amine[22] monolayers. Possible explanations for the 10° higher tilt angle in the experiments relative to these simulations include the fact that a higher pressure (1.6 GPa) was used in the experiments, or that the experiments obtained a lower coverage than the highest used in these simulations. It is worth noting that both these simulations and the in-situ AFM experiments yield a significantly larger tilt than that observed in PNR experiments of stearyl amine on iron oxide surfaces under ambient conditions ($\theta \approx 22°$)[20] because of additional tilting under compression. In these simulations, θ appears to be independent of head group and tail group type, suggesting that once the molecules are subjected to high pressure (0.5 GPa), all of the molecules pack in a similar fashion regardless of head group type or tail group Z-unsaturation. This view is supported by previous high pressure (0.3 GPa) simulations of close-packed alkanethiol monolayers on gold surfaces[44] which yielded a similar tilt angle ($\theta \approx 35°$); the slightly lower tilt angle can be rationalised through the lower applied pressure.

One might anticipate that θ would increase after sliding; however, under these simulation conditions (v_s = 10 m s^{-1}, P_z = 0.5 GPa), the average tilt angle remains very similar under both compression and sliding conditions. Rather than θ increasing, the tail groups rotate so that the molecular tilt aligns with the sliding direction, as can be observed from the average tilt orientation angle[44], Φ, defined as the orientation of the tilt angle in the *x*-*y* plane, with 0° being completely aligned with the sliding direction (*x*). At the onset of sliding, $\Phi \approx 80°$ as the tilt is aligned predominantly perpendicular to the shear. After the sliding simulations at low and medium coverage, $\Phi \approx 20°$, indicating that the tilt almost completely aligns in the sliding direction. After the sliding simulations at high coverage, $\Phi \approx 40°$, indicating partial alignment with the sliding direction, as has been noted in previous NEMD simulations of close-packed monolayers[53]. This partial alignment can be observed visually by comparing the snapshots shown in Figure 1 (compression) to Figure 3 (sliding). Longer simulations (10 ns) of high coverage SA films at v_s = 10 m s^{-1} result in the same final tilt orientation angle ($\Phi \approx$

40°), suggesting that, under these conditions, the molecular tilt is unlikely to fully align with the sliding direction regardless of the sliding time. Previous NEMD simulations have suggested that at higher sliding velocities than those studied here (>30 m s^{-1}), the shear stress may be sufficient to pull molecules in high coverage films into a completely aligned orientation[44].

The fact that θ remains similar moving from compression to sliding conditions indicates that this angle is determined solely by the film response in supporting the applied pressure, while the applied sliding simply rotates the preferred tilt orientation towards the sliding direction. The partial alignment of the molecular tilt with the sliding direction does not have a significant effect on the friction coefficient, the 100 ps block average of which remains relatively constant throughout the course of the sampling period for all of the OFMs and coverages simulated (supporting information). Indeed, a simulation with the initial tilt aligned parallel to the sliding direction (Φ ≈ 0°) yielded a friction coefficient within the statistical uncertainty of that when the initial tilt was perpendicular to the sliding direction. Previous NEMD simulations of direct monolayer-monolayer[44] and monolayer-surface[53] systems showed an increase and decrease in friction respectively when the tilt was aligned with the sliding direction. The fact that friction appears to be independent of the orientation of the tilt angle in these NEMD simulations suggests that a thin lubricant layer between the OFM films is critical in maintaining the consistent low friction observed in previous NEMD simulations[15] and boundary friction experiments[10].

Sliding Friction

The influence of surface coverage on the friction coefficient was probed at a sliding velocity, v_s = 10 m s^{-1} and a pressure, P_z = 0.5 GPa for acids, amides and glycerides (Figure 10-a). The variation in the friction coefficient with sliding velocity was also examined for acids and glycerides at a pressure, P_z = 0.5 GPa (Figure 10-b). The results indicate that the friction coefficient varies significantly with OFM coverage, head group type and sliding velocity. Figure 10-a shows that for all OFMs considered, at 10 m s^{-1} the friction coefficient at high coverage is around 30% lower than at medium coverage, and

approximately 25% less than at low coverage. Based on the structural information gathered at different coverages, this reduction in friction can be attributed to the formation of clear slip planes between the OFM films and the hexadecane lubricant, as observed through density (Figure 4), probability (Figure 5) and velocity profiles (Figure 8) as well as simulation snapshots (Figure 3). These slip planes are facilitated through the close-packing of the OFM tail groups, which leads to a solid-like, coherent monolayer film which allows very little interdigitation with the hexadecane lubricant or with each another. Indeed, large decreases in friction have also been observed for close-packed monolayers relative to loose-packed monolayers in previous NEMD simulations[24, 54] and AFM experiments[7, 55], supporting the postulate that the formation of close-packed monolayers is important for the effective friction reduction of OFMs[10].

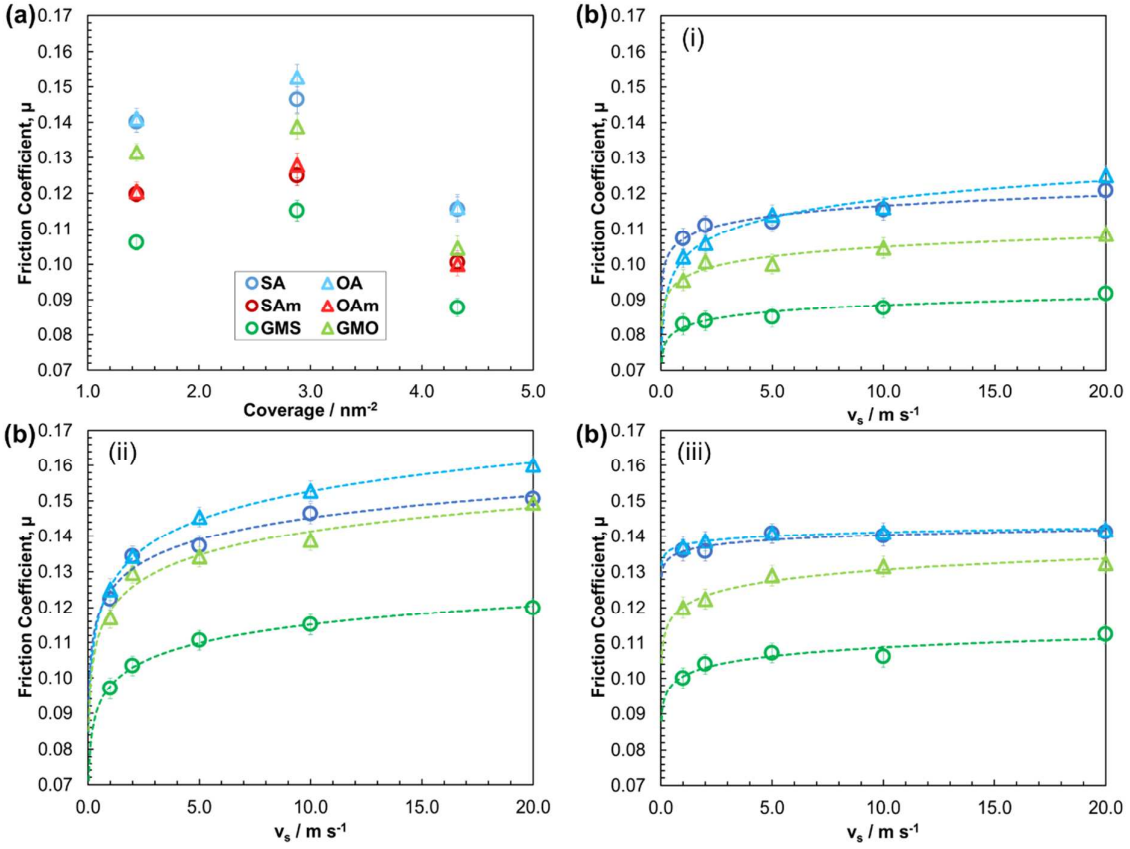


Figure 10. Friction coefficient: as a function of coverage at v_s = 10 m s^{-1} (a) and as a function of sliding velocity (b) at high coverage (i), medium coverage (ii) and low coverage (iii). Dotted line is a

logarithmic fit of the friction-velocity data for each OFM. Error bars calculated from standard deviation between block averages from 100 ps time windows.

The performance of the OFMs with respect to friction reduction is as follows: OA ≈ SA < OAm ≈ SAm ≈ GMO < GMS. As with the variation in coverage, the differences in film structure can also be used to explain the relative performance of the various OFM molecules; however, the differences are more subtle. Contrary to some previous suggestions regarding the action of glycerides as friction modifiers[56], these simulations suggest that glycerides are able to act independently as a friction modifier on steel surfaces, rather than merely serving as a reservoir for the acid. This hypothesis is supported by High Frequency Reciprocating Rig (HFRR) experimental results on steel surfaces, which showed higher friction coefficients for the di-and tri-substituted glyceride than the mono-substituted variant[2], suggesting the molecule as a whole is responsible for reducing friction, rather than its hydrolysis products. In fact, GMS is the most effective additive in reducing friction at all coverages in these simulations and this is consistent with the structural information in Figure 4 and 5, which indicate less interdigitation between the OFM film and hexadecane for glyceride compared to acid and amide, due to increased intramolecular hydrogen-bonding (Figure 7). At low coverage, the reduced friction coefficient for glycerides relative to acids and amides is probably primarily due to increased layering[51] of the OFM-hexadecane system rather than reduced interdigitation. These results agree with boundary friction experiments which have shown that amides[9] and glycerides[10] with saturated tail groups yield lower friction coefficients than acids. However, a smaller benefit of glycerides and amides relative to acids has observed experimentally than found in these simulations. This is probably due to lower glyceride and amide binding energies relative to that of the acid, which lead to lower surface coverage at equivalent concentrations; this possibility will be investigated in future adsorption experiments and DFT calculations.

In order to probe the effect on sliding velocity, v_s, on the friction of the OFM films, simulations with v_s = 1, 2, 5, 10 and 20 m s^{-1} were also conducted, as shown in Figure 10-b. The chosen sliding

velocities lie at the upper end of the range of experimentally relevant values, while still being computationally feasible and reliably thermostattable[48]. Since experimental boundary friction data on steel surfaces at different velocities are only available in the literature for acids and glycerides[10], amides are not included in these comparisons. It is noteworthy that, other than the orientation of the tilt angle mentioned previously, the film structures remained essentially unchanged through the course of the simulations over the entire range of sliding velocities simulated.

It is clear from the fitting curves in Figure 10-b that the friction coefficient increases linearly with the logarithm of the sliding velocity for all of the OFMs and coverages, in accord with experimental results[9, 10] and stress-promoted thermal activation theory[5]. The observed increase in friction with sliding velocity can be rationalized in the following way; at low velocity, as two atoms approach in the interdigitated region, they experience a repulsive force. At low sliding velocities and/or high temperatures, the molecules can adjust their geometry by thermally induced translation, rotation and conformational changes in order to avoid increasing the repulsive force as the surfaces move past one another[49]. At high sliding velocities and/or low temperatures, thermal molecular adjustment alone becomes too slow and must be increasingly augmented by shear stress promoted adjustments, so the shear stress and thus the friction coefficient increases with sliding velocity[54]. Stress-promoted thermal activation models such as this yield a linear relationship between the logarithm of sliding velocity and the friction coefficient[5, 10]. At high coverage, the barriers to interfacial sliding are small since there is very little interdigitation of the OFM film and the hexadecane lubricant (Figure 4-i), leading to a low friction coefficient which is only weakly influenced by the sliding velocity (Figure 10-b-i). This behavior mirrors that observed in SFA experiments of high coverage monolayer films of other surfactants[57]. At medium coverage, the amorphous OFM monolayers are more interdigitated by the lubricant (Figure 4-ii) and molecular adjustment is relatively slow, because molecules are closely-spaced. This means that activation barriers are both higher and more numerous, leading to a high friction coefficient which varies significantly with sliding velocity (Figure 10-b-ii). At low coverage, the film is more liquid-like and, although the films

are even more interdigitated (Figure 4-iii), the widely-spaced OFM molecules are relatively free to rearrange in order to reduce the barrier height regardless of the sliding velocity[58]. This means that low coverage films display a high friction coefficient which is almost independent of sliding velocity (Figure 10-b-iii).

At high velocity (v_s = 10 m s^{-1}), the friction coefficient increases by around 5% for all OFMs between low and medium coverage (Figure 10-a) before decreasing by 30% between medium and high coverage. This is because, at high velocity, the closely-spaced molecules in medium coverage films have insufficient time to adjust their positions without augmenting the shear stress. This pattern has been observed in SFA experiments using monolayer films formed from other surfactants in which friction increased as the film moved from a liquid-like to an amorphous film, and then decreased when a solid-like film is formed[58]. At low velocity (v_s = 1 m s^{-1}), the friction coefficient at medium coverage decreases to a value in between those at low coverage and high coverage (Figure 10-b). This is because the molecules in medium coverage films now have sufficient time to adjust their positions without significantly increasing the shear stress. Boundary friction experiments are always carried out at relatively low velocity, explaining why a steady reduction in friction is observed in these experiments when the concentration of the OFM is increased[3, 12].

The effect of tail group unsaturation on friction has been a topic of interest in many experimental[7, 8, 10] and simulation studies[16, 17] of OFMs. The current simulation results suggest that, at equal coverage, the structure (Figure 4 and 5) and friction (Figure 10) of acid and amide OFMs with Z-unsaturated tail groups are very similar to their saturated counterparts. Thus experimentally observed differences between acid and amide OFMs with saturated and Z-unsaturated tail groups are likely to have arisen from differences in their level of adsorption and thus surface coverage at the tested concentration, rather than from nanoscale structural differences. Whilst the binding energy of the OFM is not expected to change moving from saturated to Z-unsaturated tail groups[17], the 'kink' in the chain results in a larger kinetic barrier for the formation of a high coverage film due

to steric effects[19]. Indeed, in-situ AFM[13] experiments have shown that, unlike SA, OA does not form close-packed monolayers on mica surfaces at equal concentration. Similarly, SFA experiments on steel surfaces have indicated that OA is able form close-packed monolayers, but only when it is added at much higher concentrations than SA[8]. This suggests that, in boundary friction experiments[10] OFMs with saturated tail groups are more likely to form high coverage films, whilst OFMs with Z-unsaturated tail groups probably form low coverage ones. In these simulations, one can observe a 25% reduction in friction coefficient moving from low to high coverage (Figure 10-a). This level of reduction agrees well with experimentally observed differences between the friction coefficients of Z-unsaturated and saturated acid OFMs[10]. Moreover, the experimental friction coefficient for OFMs with saturated tail groups increases linearly with the logarithm of sliding velocity, whilst the friction remains almost constant for OFMs with Z-unsaturated tail groups[10]. This friction-velocity behavior is also replicated in these simulations, with the friction of high coverage (saturated) films increasing linearly with the logarithm of sliding velocity (Figure 10-b), and low coverage (unsaturated) films displaying a friction coefficient which has only a very weak dependence on sliding velocity (Figure 10-d). The simulations still show a very slight increase for low coverage films, as opposed to complete invariance observed experimentally. This difference can be explained through the possibility of a small amount of lubricant entrainment in the higher boundary friction experiment velocities[9], which, at low coverage, may be sufficient to cancel the slight increase observed in these simulations.

The influence of the tail group Z-unsaturation on glyceride OFMs is different to that for acids and amides; specifically, saturated GMS is significantly (10%) more effective in reducing friction than Z-unsaturated GMO at all coverages and sliding velocities. This is mirrored by the fact that GMS films are less interdigitated by hexadecane, as shown in in Figure 5-a, and 6-a. The cause of these differences in structure and friction is postulated to be disruption of the hydrogen-bonding network due to the ‘kink’ in the tail group.

Summary and Conclusions

In this study , classical MD simulations with an all-atom force-field have been used to investigate the structure and friction of films consisting of a range of model (SA, OA) and commercially relevant (SAm, OAm, GMS, GMO) OFMs, adsorbed on iron oxide surfaces and lubricated by a thin layer of hexadecane. The primary aim was to determine the effects of surface coverage and sliding velocity, as well as head group and tail group type, on the properties of interest. We have shown that NEMD simulations with accurate all-atom force-fields are capable of describing the structure and friction of a complex multicomponent system when care is taken in the simulation set-up. Indeed, we have found very good agreement between our results for aspects of the film structure and friction and experimental results reported in the literature.

Preliminary squeeze-out simulations demonstrate that, even at low coverage, OFM films are able to support a thin hexadecane film and prevent solid-solid contact at high pressure (P_z = 0.5 GPa). As coverage is increased, the equilibrium film thickness increases; however, the amount of lubricant trapped in this film remains constant regardless of coverage, and corresponds to two molecular layers of hexadecane. This thin layer of hexadecane appears to be critical in maintaining consistent low friction between high coverage films.

Compression simulations indicate that the OFM molecules tilt under the applied pressure (P_z = 0.5 GPa) to an extent that depends on the coverage. At low coverage, the average tilt angle was 70°, but this dropped to 40° at high coverage. The latter angle, as well as the high coverage slab separation (50-55 Å) agree well with experimental results. When sliding is applied the average tilt angle does not change significantly, but the orientation of the tilt change from being aligned perpendicular, to predominantly, though not wholly, parallel with the sliding direction.

The simulations demonstrate the key role of OFM coverage on film structure and thus on boundary friction. At low coverage the hexadecane molecules penetrate the OFM monolayers leading to a loosely ordered film that responds under shear in a viscous, almost Couette-like fashion. By

contrast, at high coverage the OFM monolayers form ordered, solid-like structures with negligible interdigitation between their methyl groups and the separating hexadecane layer. In these high coverage films shear is accommodated by slip planes between the well-defined OFM-hexadecane and hexadecane-hexadecane layers. In consequence the friction coefficient is considerably lower at high coverage than at low coverage. The medium coverage case gives an amorphous film structure which, at v_s = 10 m s^{-1}, leads to the highest friction of the three studied, since it lacks both the fluidity of the low coverage case and the clear slip plane formation that occurs at high coverage.

Amide and particularly glyceride OFMs yield lower friction coefficients than acid OFMs at all coverages in these simulations, as has been observed experimentally. This is achieved through the formation of intermolecular hydrogen-bonds between proximal head groups, which results in more coherent films, thus allowing less lubricant interdigitation. These simulations suggest that glyceride OFMs are effective in reducing friction in their own right, and thus hydrolysis to the carboxylic acid may not be required in order to reduce boundary friction, as is sometimes proposed.

A linear increase in the friction coefficient with the logarithm of the sliding velocity is confirmed for all of the OFMs at all coverages, although the dependence is greatest for medium coverage (amorphous) monolayers, and very slight in low coverage (liquid-like) monolayers. The results of the simulations suggest that differences in friction between high coverage (solid-like) and medium coverage (amorphous) OFM films will be relatively small under experimentally relevant boundary sliding velocities, while a 25% reduction is predicted when moving from low coverage to high coverage, as has been observed experimentally.

The simulation results provide strong evidence to suggest that the experimentally observed benefits of OFMs with saturated tail groups over those containing Z-unsaturation originate not primarily from the inherent structures of their films, but rather the ability to form films with a higher surface coverage. As a result, saturated OFMs should be used where possible to facilitate the formation of close-packed monolayers and maximise friction reduction in the boundary regime.

Supporting Information

Full details of the non-bonded force-field parameters as well as additional structure and friction figures are provided in the supporting information.

Acknowledgements

JPE acknowledges the financial support of the Engineering and Physical Sciences Research Council (EPSRC) via a Case Conversion studentship and Shell Global Solutions via the University Technology Centre for Fuels and Lubricants at Imperial College London. HAS, CG and DD thank the EPSRC for support under the Platform Grant EP/G026114/1. The authors also acknowledge the use of the Imperial College High Performance Computing Service for this research. URL: http://www.imperial.ac.uk/admin-services/ict/self-service/research-support/hpc/

References

(1) Spikes, H. Friction Modifier Additives. *Tribol. Lett.* **2015**, *60*, 5-5.
(2) Davidson, J. E.; Hinchley, S. L.; Harris, S. G.; Parkin, A.; Parsons, S.; Tasker, P. A. Molecular dynamics simulations to aid the rational design of organic friction modifiers. *J. Mol. Graphics Modell.* **2006**, *25*, 495-506.
(3) Jahanmir, S.; Beltzer, M. An adsorption model for friction in boundary lubrication. *ASLE Trans.* **1986**, *29*, 423-430.
(4) Beltzer, M.; Jahanmir, S. Role of dispersion interactions between hydrocarbon chains in boundary lubrication. *ASLE Trans.* **1987**, *30*, 47-54.
(5) Briscoe, B. J.; Evans, D. C. B. The shear properties of Langmuir-Blodgett layers. *Proc. R. Soc. A* **1982**, *380*, 389.
(6) Jahanmir, S. Chain-length effects in boundary lubrication. *Wear* **1985**, *102*, 331-349.
(7) Ruths, M.; Lundgren, S.; Danerlov, K.; Persson, K. Friction of fatty acids in nanometer-sized contacts of different adhesive strength. *Langmuir* **2008**, *24*, 1509-1516.
(8) Lundgren, S. M.; Ruths, M.; Danerlov, K.; Persson, K. Effects of unsaturation on film structure and friction of fatty acids in a model base oil. *J. Colloid Interface Sci.* **2008**, *326*, 530-536.
(9) Ingram, M.; Noles, J.; Watts, R.; Harris, S.; Spikes, H. A. Frictional Properties of Automatic Transmission Fluids: Part I-Measurement of Friction-Sliding Speed Behavior. *Tribol. Trans.* **2011**, *54*, 145-153.
(10) Campen, S.; Green, J.; Lamb, G.; Atkinson, D.; Spikes, H. On the Increase in Boundary Friction with Sliding Speed. *Tribol. Lett.* **2012**, *48*, 237-248.
(11) Campana, M.; Teichert, A.; Clarke, S.; Steitz, R.; Webster, J. R. P.; Zarbakhsh, A. Surfactant Adsorption at the Metal-Oil Interface. *Langmuir* **2011**, *27*, 6085-6090.
(12) Simic, R.; Kalin, M. Comparison of Alcohol and Fatty Acid Adsorption on Hydrogenated DLC Coatings Studied by AFM and Tribological Tests. *Stroj. Vestn.-J. Mech. E.* **2013**, *59*, 707-718.
(13) Campen, S.; Green, J. H.; Lamb, G. D.; Spikes, H. A. In Situ Study of Model Organic Friction Modifiers Using Liquid Cell AFM; Saturated and Mono-unsaturated Carboxylic Acids. *Tribol. Lett.* **2015**, *57*, 20.
(14) Luo, H.; Fan, W. Y.; Li, Y.; Zhao, P. H.; Nan, G. Z. Experimental and Molecular Dynamics Simulations for Investigating the Effect of Fatty Acid and Its Derivatives on Low Sulfur Diesel Lubricity. *China Pet. Process. Petrochem. Technol.* **2013**, *15*, 79-85.
(15) Eder, S. J.; Vernes, A.; Betz, G. On the Derjaguin Offset in Boundary-Lubricated Nanotribological Systems. *Langmuir* **2013**, *29*, 13760-13772.
(16) Doig, M.; Warrens, C. P.; Camp, P. J. Structure and Friction of Stearic Acid and Oleic Acid Films Adsorbed on Iron Oxide Surfaces in Squalane. *Langmuir* **2014**, *30*, 186-195.
(17) Loehle, S.; Matta, C.; Minfray, C.; Le Mogne, T.; Martin, J. M.; Iovine, R.; Obara, Y.; Miura, R.; Miyamoto, A. Mixed Lubrication with C18 Fatty Acids: Effect of Unsaturation. *Tribol. Lett.* **2014**, *53*, 319-328.
(18) Loehle, S.; Matta, C.; Minfray, C.; Le Mogne, T.; Iovine, R.; Obara, Y.; Miyamoto, A.; Martin, J. M. Mixed lubrication of steel by C18 fatty acids revisited. Part I: Toward the formation of carboxylate. *Tribol. Int.* **2015**, *82*, 218-227.
(19) Loehle, S.; Matta, C.; Minfray, C.; Le Mogne, T.; Iovine, R.; Obara, Y.; Miyamoto, A.; Martin, J. M. Mixed lubrication of steel by C18 fatty acids revisited. Part II: Influence of some key parameters. *Tribol. Int.* **2016**, *94*, 207-216.
(20) Wood, M. H.; Welbourn, R. J. L.; Charlton, T.; Zarbakhsh, A.; Casford, M. T.; Clarke, S. M. Hexadecylamine Adsorption at the Iron Oxide-Oil Interface. *Langmuir* **2013**, *29*, 13735-13742.
(21) Doig, M.; Camp, P. J. The structures of hexadecylamine films adsorbed on iron-oxide surfaces in dodecane and hexadecane. *Phys. Chem. Chem. Phys.* **2015**, *17*, 5248-5255.
(22) Campen, S.; Green, J. H.; Lamb, G. D.; Spikes, H. A. In Situ Study of Model Organic Friction Modifiers Using Liquid Cell AFM: Self-Assembly of Octadecylamine. *Tribol. Lett.* **2015**, *58*, 39-39.

(23) Casford, M. T. L.; Davies, P. B. The Structure of Oleamide Films at the Aluminum/Oil Interface and Aluminum/Air Interface Studied by Sum Frequency Generation (SFG) Vibrational Spectroscopy and Reflection Absorption Infrared Spectroscopy (RAIRS). *ACS Appl. Mater. Interfaces* **2009**, *1*, 1672-1681.
(24) Chandross, M.; Webb, E. B.; Stevens, M. J.; Grest, G. S.; Garofalini, S. H. Systematic study of the effect of disorder on nanotribology of self-assembled monolayers. *Phys. Rev. Lett.* **2004**, *93*, 4.
(25) Pastewka, L.; Moser, S.; Moseler, M. Atomistic Insights into the Running-in, Lubrication, and Failure of Hydrogenated Diamond-Like Carbon Coatings. *Tribol. Lett.* **2010**, *39*, 49-61.
(26) Li, Q. Y.; Dong, Y. L.; Perez, D.; Martini, A.; Carpick, R. W. Speed Dependence of Atomic Stick-Slip Friction in Optimally Matched Experiments and Molecular Dynamics Simulations. *Phys. Rev. Lett.* **2011**, *106*, 4.
(27) Plimpton, S. Fast parallel algorithms for short-range molecular-dynamics. *J. Comput. Phys.* **1995**, *117*, 1-19.
(28) Maslen, E. N.; Streltsov, V. A.; Streltsova, N. R.; Ishizawa, N. Synchrotron X-ray study of the electron-density in alpha-Fe2O3. *Acta Crystallogr., Sect. B: Struct. Sci.* **1994**, *50*, 435-441.
(29) Ramachandran, S.; Tsai, B. L.; Blanco, M.; Chen, H.; Tang, Y. C.; Goddard, W. A. Self-assembled monolayer mechanism for corrosion inhibition of iron by imidazolines. *Langmuir* **1996**, *12*, 6419-6428.
(30) Kawaguchi, M.; Yamamoto, M.; Nakamura, T.; Yamashita, M.; Kato, T. Surface properties of mono-, di-, and triglycerol monostearate monolayers spread at the air-water interface. *Langmuir* **2001**, *17*, 4677-4680.
(31) Jorgensen, W. L.; Maxwell, D. S.; TiradoRives, J. Development and testing of the OPLS all-atom force field on conformational energetics and properties of organic liquids. *J. Am. Chem. Soc.* **1996**, *118*, 11225-11236.
(32) Price, M. L. P.; Ostrovsky, D.; Jorgensen, W. L. Gas-phase and liquid-state properties of esters, nitriles, and nitro compounds with the OPLS-AA force field. *J. Comput. Chem.* **2001**, *22*, 1340-1352.
(33) Siu, S. W. I.; Pluhackova, K.; Bockmann, R. A. Optimization of the OPLS-AA Force Field for Long Hydrocarbons. *J. Chem. Theory Comput.* **2012**, *8*, 1459-1470.
(34) Murzyn, K.; Bratek, M.; Pasenkiewicz-Gierula, M. Refined OPLS All-Atom Force Field Parameters for n-Pentadecane, Methyl Acetate, and Dimethyl Phosphate. *J. Phys. Chem. B* **2013**, *117*, 16388-16396.
(35) Yeh, I. C.; Berkowitz, M. L. Ewald summation for systems with slab geometry. *J. Chem. Phys.* **1999**, *111*, 3155-3162.
(36) Berro, H.; Fillot, N.; Vergne, P. Molecular dynamics simulation of surface energy and ZDDP effects on friction in nano-scale lubricated contacts. *Tribol. Int.* **2010**, *43*, 1811-1822.
(37) Ryckaert, J. P.; Ciccotti, G.; Berendsen, H. J. C. Numerical-integration of Cartesian equations of motion of a system with constraints - molecular-dynamics of n-alkanes. *J. Comput. Phys.* **1977**, *23*, 327-341.
(38) Schneider, T.; Stoll, E. Molecular-dynamics study of a three-dimensional one-component model for distortive phase-transitions. *Phys. Rev. B* **1978**, *17*, 1302-1322.
(39) Gattinoni, C.; Mackowiak, S.; Heyes, D. M.; Branka, A. C.; Dini, D. Boundary-controlled barostats for slab geometries in molecular dynamics simulations. *Phys. Rev. E* **2014**, *90*, 13.
(40) Sivebaek, I. M.; Samoilov, V. N.; Persson, B. N. J. Squeezing molecular thin alkane lubrication films between curved solid surfaces with long-range elasticity: Layering transitions and wear. *J. Chem. Phys.* **2003**, *119*, 2314-2321.
(41) Persson, B. N. J.; Mugele, F. Squeeze-out and wear: fundamental principles and applications. *J. Phys. Condens. Matter* **2004**, *16*, R295-R355.
(42) Gosvami, N. N.; Sinha, S. K.; Hofbauer, W.; O'Shea, S. J. Solvation and squeeze out of hexadecane on graphite. *J. Chem. Phys.* **2007**, *126*, 5.

(43) Salacuse, J. J.; Denton, A. R.; Egelstaff, P. A. Finite-size effects in molecular dynamics simulations: Static structure factor and compressibility .1. Theoretical method. *Phys. Rev. E* **1996**, *53*, 2382-2389.
(44) Ramin, L.; Jabbarzadeh, A. Frictional properties of two alkanethiol self assembled monolayers in sliding contact: Odd-even effects. *J. Chem. Phys.* **2012**, *137*.
(45) Humphrey, W.; Dalke, A.; Schulten, K. VMD: Visual molecular dynamics. *J. Mol. Graphics Modell.* **1996**, *14*, 33-38.
(46) Liem, S. Y.; Brown, D.; Clarke, J. H. R. Investigation of the homogeneous-shear nonequilibrium-molecular-dynamics method. *Phys. Rev. A* **1992**, *45*, 3706-3713.
(47) Bernardi, S.; Todd, B. D.; Searles, D. J. Thermostating highly confined fluids. *J. Chem. Phys.* **2010**, *132*, 10.
(48) Toton, D.; Lorenz, C. D.; Rompotis, N.; Martsinovich, N.; Kantorovich, L. Temperature control in molecular dynamic simulations of non-equilibrium processes. *J. Phys. Condens. Matter* **2010**, *22*, 12.
(49) He, G.; Robbins, M. O. Simulations of the kinetic friction due to adsorbed surface layers. *Tribol. Lett.* **2001**, *10*, 7-14.
(50) Greenfield, M. L.; Ohtani, H. Packing of simulated friction modifier additives under confinement. *Langmuir* **2005**, *21*, 7568-7578.
(51) Savio, D.; Fillot, N.; Vergne, P. A Molecular Dynamics Study of the Transition from Ultra-Thin Film Lubrication Toward Local Film Breakdown. *Tribol. Lett.* **2013**, *50*, 207-220.
(52) McDonald, I. K.; Thornton, J. M. Satisfying hydrogen-bonding potential in proteins. *J. Mol. Biol.* **1994**, *238*, 777-793.
(53) Mikulski, P. T.; Gao, G.; Chateauneuf, G. M.; Harrison, J. A. Contact forces at the sliding interface: Mixed versus pure model alkane monolayers. *J. Chem. Phys.* **2005**, *122*, 9.
(54) Kong, Y. C.; Tildesley, D. J.; Alejandre, J. The molecular dynamics simulation of boundary-layer lubrication. *Mol. Phys.* **1997**, *92*, 7-18.
(55) Lee, D. H.; Oh, T.; Cho, K. Combined effect of chain length and phase state on adhesion/friction behavior of self-assembled monolayers. *J. Phys. Chem. B* **2005**, *109*, 11301-11306.
(56) Tang, Z. L.; Li, S. H. A review of recent developments of friction modifiers for liquid lubricants (2007-present). *Curr. Opin. Solid State Mater. Sci.* **2014**, *18*, 119-139.
(57) Mazuyer, D.; Cayer-Barrioz, J.; Tonck, A.; Jarnias, F. Friction dynamics of confined weakly adhering boundary layers. *Langmuir* **2008**, *24*, 3857-3866.
(58) Yoshizawa, H.; Chen, Y. L.; Israelachvili, J. Fundamental mechanisms of interfacial friction: 1. relation between adhesion and friction. *J. Phys. Chem.* **1993**, *97*, 4128-4140.

Table of Contents Figure

